Journal of Electroanalytical Chemistry 815 (2018) 8–15

Contents lists available at ScienceDirect

Journal of Electroanalytical Chemistry

journal homepage: www.elsevier.com/locate/jelechem

Electrochemical deposition and anodic stripping of PdZn bimetallic compound

R.J. Morelock[a], W.D. Sides[a], Y. Hu[a], Q. Huang[a,b,*]

[a] Department of Chemical and Biological Engineering, University of Alabama, Tuscaloosa 35487, United States
[b] Center of Materials for Information Technology, University of Alabama, Tuscaloosa 35487, United States

ARTICLE INFO

Keywords:
Palladium zinc alloy
Bimetallic compound
Electrodeposition
Anodic stripping
Underpotential codeposition

ABSTRACT

Pd alloys with non-noble transition metals are of interest for various catalytic applications. The electrodeposition of Pd-Zn alloy was investigated from an ammonia citrate electrolyte at neutral pH in this report. Cyclic voltammetry, galvanostatic deposition, and potentiostatic stripping were used to understand the electrochemical behavior of the system. Films were characterized with electron microscopy, X-ray diffraction, Raman spectroscopy and X-ray photoelectron spectroscopy. While Zn-rich alloy films with various compositions were electrodeposited at different current densities, a porous but stable tetragonal PdZn bimetallic compound was obtained after anodic stripping.

1. Introduction

Pd alloys with different transition metals have been studied as alternatives to pure Pd or Pt as catalyst in a variety of chemical and electrochemical processes. For example, alloying Pd with Fe was found to improve the selectivity of hydrogen production during the decomposition of methane [1]. PdNi has been recently investigated as the electrocatalyst for oxidation of methanol, where the resistance to fuel poisoning was improved as a result of weaker affinity with carbonaceous byproducts [2,3]. In addition, Pd-Zn alloy catalysts have been studied for hydrogenation [4–7] and steam reforming of methanol [8–11]. A recent article reported an improved ethanol oxidation performance for porous PdAgZn alloys created by electrodepositing Zn on PdAg foils and partially dissolving Zn from the annealed alloy [12].

While the electrodeposition of Pd alloys with Ni and Fe has been reported in the past [13–15], studies on the co-deposition of Pd and Zn are very limited. A literature study only resulted in two short communications [16,17], where Pd-Zn alloys with low Zn content (max. < 25 at.%) were co-deposited. Due to the big difference in reversible potential of Pd and Zn, various complexing agents were used to chelate Pd cations and to bring the potentials closer. However, the much high nobility of Pd dictated a low content of Zn in the alloy [16,17].

As electrodeposition is typically a highly-biased process at low temperature, it is capable of producing metastable materials, namely materials not at thermodynamic equilibrium states. On the other hand, formation of compounds with a well-defined stoichiometry and crystalline phase has been relatively less available. While bulk deposition of compound materials, such as CuInSe [18–23], CoSe [24] and SbTe [25–27], were also reported, they were deposited rather as an alloy. The compositions of such alloys were tunable with the process and were often off-stoichiometry. A well-known case of stoichiometric compound from electrodeposition is CdTe [28], where Cd was deposited as a result of formation of CdTe compound, causing a underpotential deposition (UPD) of Cd with Te. The formation of stoichiometric compound relies on a charge transfer between the metal and chalcogen elements, resulting in a large free energy of formation of stoichiometric compounds. Similar deposition was reported for some other chalcogenide compounds [29–35]. Another type of UPD process that has been extensively explored is for layer-by-layer electrodeposition of compounds [36–42] and metals [43–47]. While the under-potentially deposited element is a part of the compound itself in the former case, it is used as an intermediate to exchange for the desired element in the latter.

This paper reports a study of the electrodeposition of Zn-rich Pd-Zn alloys, where an additional anodic stripping was used to remove excessive Zn and achieve stoichiometric bimetallic compounds. The interactions between two elements during electrodeposition and the effects of process on the composition, morphology and crystal structure of deposit are studied.

2. Experimental

2.1. Electrochemical cell

Electrodeposition was carried out in a three-electrode cell, where a

* Corresponding author at: Department of Chemical and Biological Engineering, University of Alabama, Tuscaloosa, 35487, United States.
E-mail address: qhuang@eng.ua.edu (Q. Huang).

https://doi.org/10.1016/j.jelechem.2018.03.003
Received 12 January 2018; Received in revised form 28 February 2018; Accepted 1 March 2018
Available online 02 March 2018

zinc rod was used as anode and Ag/AgCl electrode as the reference. The cathode was a disc electrode rotating at 400 rpm. An Autolab 302 N electrochemical station was used for all the electrochemical studies. The positions of the three electrodes were fixed for all the experiments. All voltages are referred with respect to Ag/AgCl in this report.

A non-exchangeable platinum (Pt) disc electrode was used in cyclic voltammetry study, which allows the anodic stripping of palladium (Pd). Exchangeable molybdenum (Mo) and copper (Cu) disc electrodes were used to prepare films for characterization. The X-ray peak of copper is close to zinc and the use of copper disc was found to cause an underestimate of zinc content in the films. On the other hand, Mo results in an x-ray diffraction peak that overlaps with Pd-Zn alloys. Therefore, Mo disc was used to deposit films for compositional analysis and Cu disc was used for other film analysis. While the substrate is expected to make a difference in the initial nucleation of deposit, such effects is believed to be negligible on the overall film deposition after the nucleation. All disc electrodes were polished on a series of sand paper and aluminum oxide particles down to 50 nm.

2.2. Cathodic deposition and anodic stripping

The electrolyte used is composed of 3 mM $PdCl_2$, 0.3 M $ZnCl_2$, 0.4 M Citric Acid, and 1.3 M NH_3. The pH of the solution was adjusted to 7 using dilute HCl and KOH. Films were deposited at different current densities from -5 to -25 mA/cm^2. A constant charge of 0.9 C/cm^2 was used to control the time of deposition, which corresponds to 425 nm at 100% cathodic current efficiency. For stripping experiments, the electrodes with electrodeposited alloys were cleaned with DI water. They were then rotated at 400 rpm, and subjected to an applied potential of -0.5 V for 30 s (or until a constant current was achieved). The same electrolyte for deposition was used for the stripping study because it potentially provides a way of doing in-situ stripping with a pulse reverse scheme in the future.

2.3. Film characterization

The compositions and thicknesses of the electrodeposited and anodically stripped Pd-Zn alloys were determined with X-ray fluorescence (XRF). The morphology of films was characterized with a JEOL 7000 field emission scanning electron microscope (SEM). The crystallographic structures were characterized with Bruker D8 X-ray diffractometer (XRD) using Co Kα source with a wavelength of 1.79 Å. Raman spectra were acquired with Hiroba Jobin Yvon Raman microscope with a Laser Quantum Ventus 1064 laser source at a wavelength of 532 nm. A Kratos Axis 165 X-ray photoelectron spectrometer (XPS) was acquired to characterize the binding energy of Pd3d and Zn2p electrons in the films. Carbon peaks were used to calibrate the peak positions for all XPS spectra.

3. Results and discussion

3.1. Characterization of the electrochemical system

Cyclic voltammetry (CV) with various potential windows were carried out on Pt disc to understand the electrochemical behaviors of the elements. Fig. 1 shows the comparison of the CV studies between alloy and elemental electrolytes. The potential was swept down to -0.5 V the first CV in Fig. 1(a). A small cathodic current was observed below a potential of -0.06 V, reaching a plateau of -0.25 mA/cm^2. One current peak was observed at 0.63 V and is assigned to the anodic dissolution of pure Pd. As the potential was swept to more negative potentials, i.e., -0.7 V, in Fig. 1(b), a sharp increase of cathodic current was observed. This cathodic current resulted in another anodic current peak on the reverse scan. This pair of cathodic-anodic current seems to have a reversible potential at -0.55 V and is believed to be the adsorption and desorption of hydrogen. More discussion on this conclusion will be provided in the discussions in the anodic stripping sections. While an additional cathodic current peak was observed later indicating the saturation of hydrogen adsorption, no further change was observed on the CVs other than the increase of the peak heights as more and more Pd was deposited. On the other hand, no Zn deposition was observed down to -1.1 V. Anodic dissolution of Zn was observed in Fig. 1(e), where a negative potential of -1.3 V was reached.

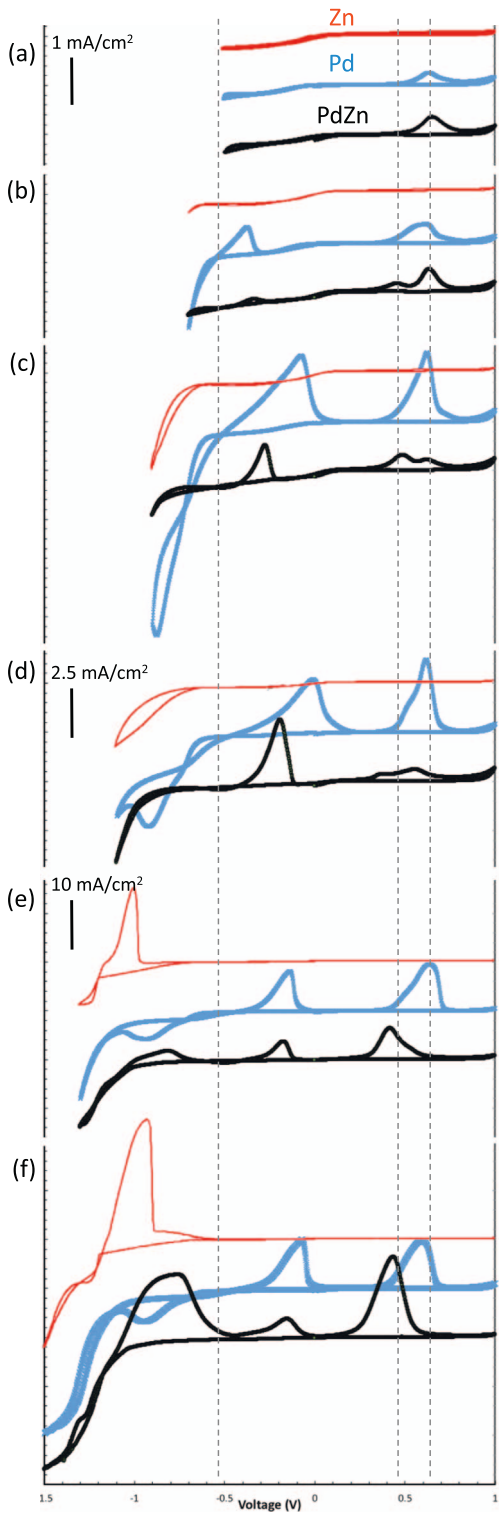

Fig. 1. Cyclic voltammograms with different sweep potential windows acquired in the ammonia-citrate Pd Zn alloy electrolyte on Pt disc electrode at a rotation rate of 400 rpm.

The CV of Pd-Zn alloy electrolyte behaves exactly the same as the elemental Pd electrolyte down to −0.5 V, where only pure Pd was deposited and stripped at 0.63 V. When the voltage was further decreased to −0.7 V, a second anodic stripping peak was observed at 0.45 V. At the same time, the stripping peak of pure Pd decreased. Therefore, a Pd-Zn alloy or compound was believed to have formed. The anodic peak at 0.45 is believed to be the stripping of this compound rather than the Zn itself. As discussed above, zinc deposition does not start until at −1.3 V in elemental zinc electrolyte, the formation of Pd-Zn alloy at −0.7 V indicates an underpotential deposition of Zn. At the same time, the hydrogen desorption peak is much smaller than pure Pd case, suggesting the solubility of hydrogen is much lower due to the mixing of Zn. As the CV further extended to more negative than −1.3 V, an additional stripping peak for pure Zn was observed. The stripping of Pd-Zn alloy became more dominant than pure Pd. In addition, the hydrogen desorption peak does not increase anymore and of same size for the case with CV down to −1.1 V. All these observations suggested that no Pd was deposited at potentials more negative than −1.1 V and all the deposit was Pd-Zn alloy and pure Zn.

The speciation of metal ions and chelating agents can be calculated with the stability constants of different species [48]. The complexing reactions and stability constants used in the calculation are listed in Table S1 in Supporting Materials. Fig. 2 shows the fractions of different metal chelates with respect to the total metal concentrations at different solution pH's for Pd-Zn alloy solution. While various types of Zn(II) complexes with citrate anions are present at different pH's below 7, Pd and Zn are completely present as $[Pd(NH_3)_4]^{2+}$ and $[Zn(NH_3)_4]^{2+}$, respectively, when pH is 7 or above. The formation of zincate anions is not expected due to the presence of abundant NH_3. Complexed metal ions with lower coordination numbers are negligible for both Pd and Zn. While the ammonia complexed with Pd^{2+} is negligible due to the much lower total concentration of Pd(II), the majority of ammonia is used to complex with Zn^{2+} at pH above 6. The rest of ammonia is present as NH_4^+ between pH 6 and 8 and as NH_3 at pH above 10. On the other hand, all citric acid is present as citrate anion at pH above 7.

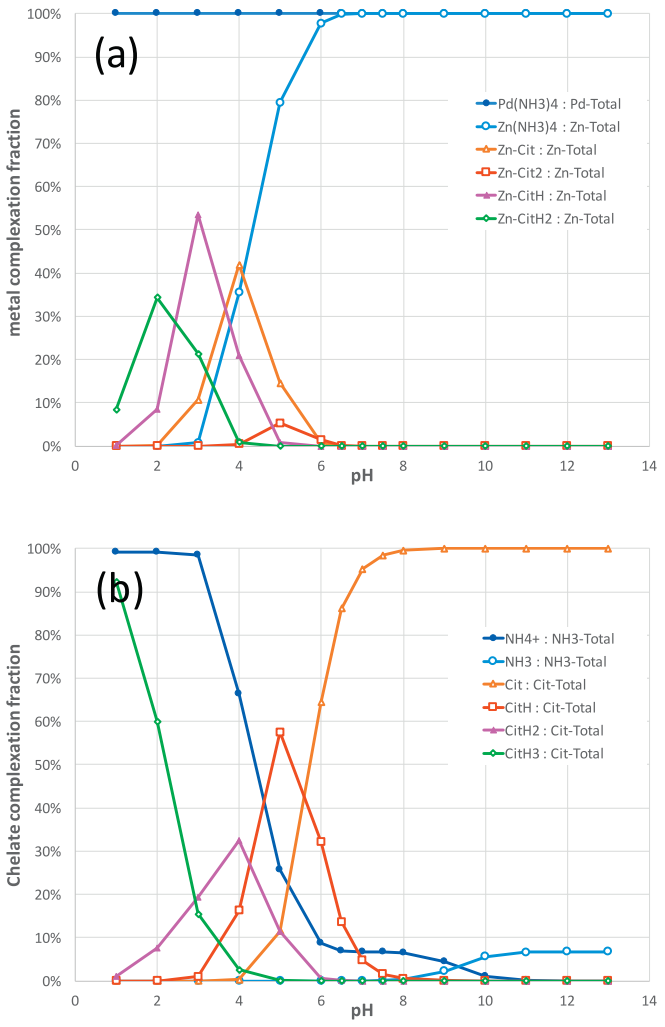

Fig. 2. The change of speciation at different solution pH's for (a) Pd and Zn metal cations; (b) ammonia and citrate chelating agents.

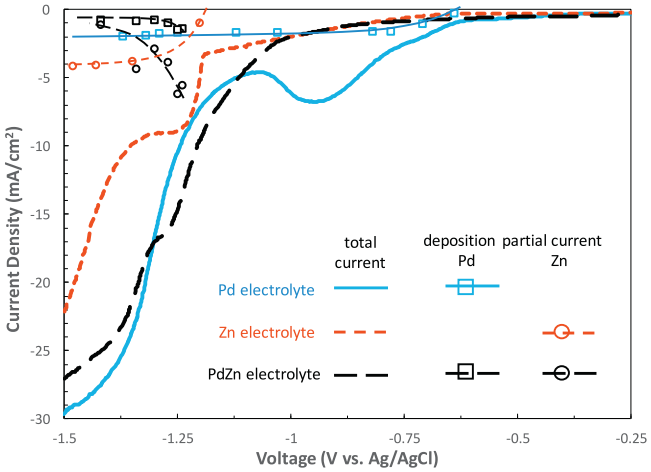

Fig. 3. The linear sweep voltammetry and partial current densities of metal deposition of elemental Pd, elemental Zn, and Pd-Zn alloy electrolytes obtained on Mo disc electrode at a rotation rate of 400 rpm.

Galvanostatic deposition was carried out at various total current densities from elemental and alloy electrolytes. The thickness and composition of the deposited films were analyzed with XRF and were used to calculate the partial current densities. Fig. 3 shows the total current densities and partial current densities for the different electrolytes. Pure Pd electrolyte resulted in the highest total current density, probably due to the catalytic effect of Pd on hydrogen evolution reaction. A diffusion limited Pd deposition partial current density of $-1.7\ mA/cm^2$ was clearly observed, corresponding to a deposition rate of 0.78 nm/s. Using Levich's equation [49], a diffusion coefficient of 9.2E-7 cm^2/s was obtained for $[Pd(NH_3)_4]^{2+}$ in this electrolyte, which is significantly lower than most simple metal cations [50].

On the other hand, Zn deposition partial current starts at −1.2 V. A current plateau was also observed at $-4.17\ mA/cm^2$, corresponding to a diffusion coefficient of 3.6E-9 cm^2/s for $[Zn(NH_3)_4]^{2+}$ if it is the limiting current density of the reduction of $[Zn(NH_3)_4]^{2+}$. This diffusion coefficient is dramatically lower than Zn^{2+} in acidic solutions as well as the complexed $[Pd(NH_3)_4]^{2+}$ in the same electrolyte. Therefore, it is very likely that the current plateau observed is not due to the reduction of $[Zn(NH_3)_4]^{2+}$ but some other complexed Zn species. The detailed concentrations of different species between pH 6 to 7.5 are listed in Table S2 in Supporting Materials. While the results were listed for alloy electrolyte, the presence of 3 mM Pd(II) in the alloy solution does not change the Zn complexation from Zn-only electrolyte. It is evident that zincate ions are negligible even at a high pH of 13 due to the complexation with NH_3. The only available Zn cations are $[Zn\text{-}Cit]^-$ and $[Zn\text{-}Cit_2]^{4-}$, of which the total concentration is negligible at a pH of 7, but reaches 0.3 mM and 6.7 mM at a pH of 6.5 and 6, respectively. At a total concentration of 6.7 mM, the diffusion coefficients of $[Zn\text{-}Cit]^-$ and $[Zn\text{-}Cit_2]^{4-}$ calculated from the current plateau would be 1.1E-6 cm^2/s, which is in the same range of $[Pd(NH_3)_4]^{2+}$. While the pH of solution is not expected to drop significantly to 6, this discrepancy in diffusion coefficient is believed to result from the

uncertainty in some stability constants as well as a small pH deviation of solution.

On the other hand, the reversible potential of the two complexed Zn-citrate cations can be estimated from the stability constants and Nernst equation as follows: $E_{rev} = E^{\ominus} - 0.029\ pK_{st} + 0.029\ log_{10}(C_{ox})$. With a standard potential of −0.96 V (vs. Ag/AgCl) for Zn^{2+}, the stability constants of 5.0 for $[Zn\text{-}Cit]^-$ and 5.9 for $[Zn\text{-}Cit_2]^{4-}$, and the concentrations of 2.2 mM for $[Zn\text{-}Cit]^-$ and 4.5 mM for $[Zn\text{-}Cit_2]^{4-}$, the reversible potentials are estimated as −1.18 V for $[Zn\text{-}Cit]^-$ and −1.20 V for $[Zn\text{-}Cit_2]^{4-}$ (vs. Ag/AgCl). This estimate is consistent with the observation in CV (Fig. 1) and the partial current (Fig. 3), also suggesting that the Zn deposition was due to the reduction of $[Zn\text{-}Cit]^-$ and $[Zn\text{-}Cit_2]^{4-}$.

The partial current densities of Pd deposition from Pd-Zn alloy electrolyte was lower than in the elemental Pd electrolyte. This inhibition of the more noble Pd element is similar to the so called anomalous codeposition [51–54], but it is here resulted from the underpotential co-deposition of Zn and relates to a much lower work function of Zn than Pd [55–57]. At the same time, Zn deposition in Pd-Zn alloy system was enhanced as compared with Zn-only electrolyte at potentials above −1.5 V, consistent with the underpotential co-deposition observed in the CV studies. However, because the Zn deposition rate was even higher than the limiting current density observed in the elemental Zn electrolyte, it is believed that reduction of other Zn cations also occurred due to this promotive effect of co-deposition.

The deposition rate of Zn in alloy system significantly decreases as the deposition potential became more negative. This is probably due to the catalytic hydrogen evolution reaction in presence of Pd and a significant pH increase at cathode surface, resulting in a change of speciation. It can be seen from Fig. 2 and Table S2 in Supporting Materials that Zn-citrate species quickly disappears as pH increases. At the same time, the strongly complexed $[Zn(NH_3)_4]^{2+}$ would not be reduced until at more negative potentials, resulting in the current decrease.

3.2. Anodic stripping of deposited films

The CVs of Pd-Zn alloy system in Fig. 1 showed both anodic stripping or desorption processes at various potentials. Different alloy films were deposited at different current densities up to a constant charge 900 mC/cm^2. As presented in Fig. 4, the as-deposited films are Zn-rich. The Zn contents increases with the deposition current densities, consistent with the elemental Zn deposition observed in CVs at more negative potentials. Anodic stripping was therefore carried out at −0.5 V for 30 s for three Pd-Zn alloy films, which were deposited at −15, −20, and −25 mA/cm^2, respectively. Zn contents of the films fall between 40

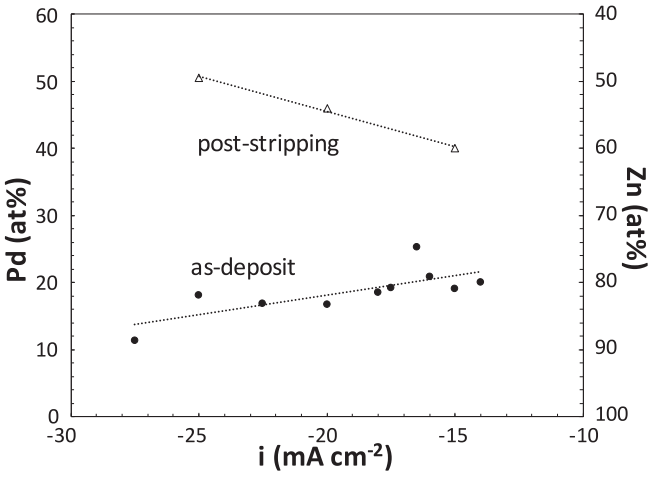

Fig. 4. Compositions of Pd-Zn alloy films deposited at different current densities before and after anodic stripping.

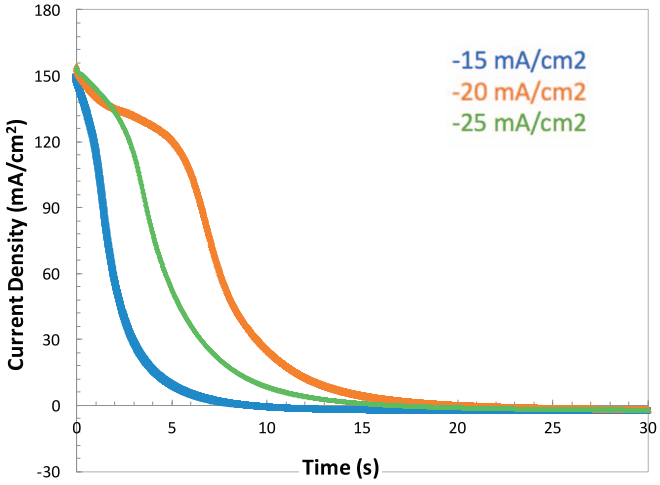

Fig. 5. The current density evolution during the anodic stripping at −0.5 V (Ag/AgCl) of three Pd-Zn alloy films deposited at −15, −20, and −25 mA/cm^2.

at.% and 60 at.% after stripping.

Fig. 5 shows the current evolution along the stripping of the same three films in Fig. 4. A high anodic current density was observed at the beginning and this stripping current decays to zero for all three films. In fact, the final current density was a small cathodic current, consistent with the steady state cathodic deposition of Pd observed in CV at −0.5 V. The amount of Pd deposition is believed to be negligible due to the low current density and short time. Anodic Stripping lasted for different time for the films, depending on the different thicknesses. Because all the films after stripping had a composition between 40 and 60 at.% Zn, a stable bimetallic phase is believed to form. In addition, a second stripping attempt at 0 V didn't resolve any anodic current, further confirming that the films after the first stripping was stable and do not have excessive Zn that can be stripped. The binary Pd-Zn phase diagram [58] shows that an intermetallic compound phase forms at a composition range between 40 and 60 at.% Zn, consistent with the observation here. While a typical stripping process can only remove elements on the electrode surface, a de-alloy process can create porous films that allows the continuous removal of elements beneath the surface.

3.3. Characterization of films

Fig. 6 shows the morphology of films galvanostatically deposited at various current densities for 900 mC/cm^2 before and after anodic stripping. Continuous films with smooth surface and metallic luster were obtained at a current density of −15 mA/cm^2 or above. The film deposited at −10 mA/cm^2 was also of metallic luster but was not continuous under SEM inspection. Shallow grooves from mechanical polishing of the disc electrode were sometimes observed. Porous patches and cracks on the scale of a micron were observed on the same films after stripping. EDS mapping in Fig. S3 in Supporting Materials showed that the patched regions, for example the region labeled as "A" in Fig. 6(a′) has a much stronger signal from copper substrate, suggesting a much thinner Pd-Zn film. This suggests that the composition in the as-deposit Pd-Zn film was not uniform. Regions with a higher Zn content were stripped to a more degree than regions with a lower Zn content. This non-uniformity in stripping was observed in all the films deposited at various current densities.

The crystallographic structures of the films were characterized XRD and the results are shown in Fig. 7. Electrodeposited pure Zn and pure Pd films were also included for comparison. Other than the film deposited at −10 mA/cm^2 didn't show distinct peaks due to the limited film thickness, strong XRD reflections were observed for films deposited at higher current densities. As discussed above, the Zn contents in the

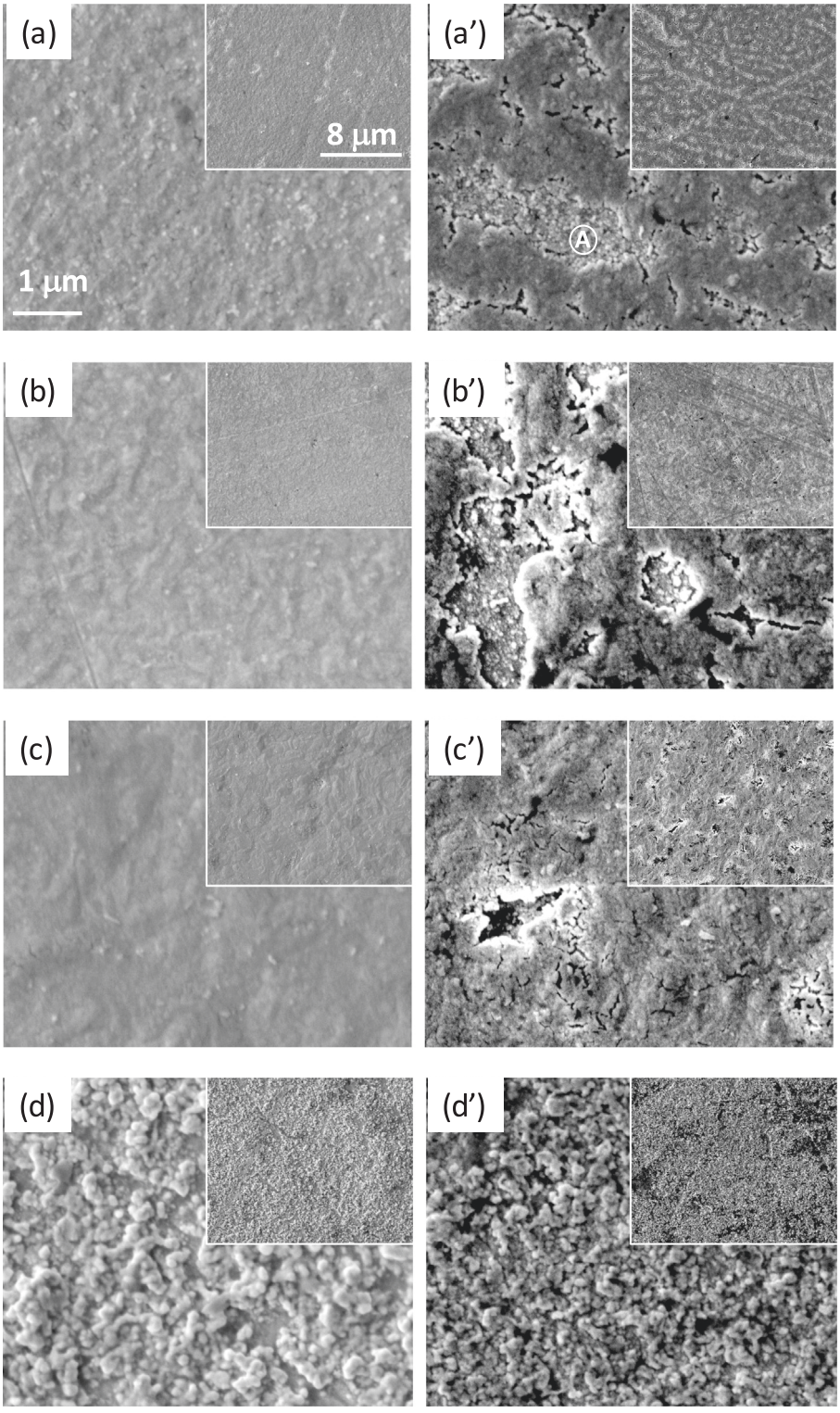

Fig. 6. Topdown SEM images of the surface morphology of Pd-Zn alloy films deposited at (a, a′) −25, (b, b′) −20, (c, c′) −15, and (d, d′) −10 mA/cm^2. (a–d) before and (a′–d′) after anodic stripping at −0.5 V.

as-deposit films were above 66 at.%. However, such Pd-Zn alloys were of the orthorhombic $PdZn_2$ phase. No reflections of hexagonal Zn or cubic Pd phase were detected. A strong doublet peak was observed at 2θ of 47.6° and at 48.2°, corresponds to the preferred crystalline orientations. While the first peak corresponds to the (312) or (223) reflections of orthorhombic $PdZn_2$, the second peak relates to the (132) reflection. The other two reflections observed at 67.2° and 92.0° result from the (422) and (352) phases.

The crystalline structure of the films was completely changed after the anodic stripping. As shown in Fig. 7(b), only one reflection was observed at 47.7°. While this peak can be the first peak in the aforementioned doublet, it can also be assigned to the (111) reflection of Pd-Zn. Since all the other reflections of Pd-Zn_2 disappeared after stripping and the alloy composition is at about 50% Zn, this reflection is believed to be (111) reflection of Pd-Zn. The FWHM of this reflection was 0.21°, 0.47°, and 0.42° (after the correction of instrumental broadening of

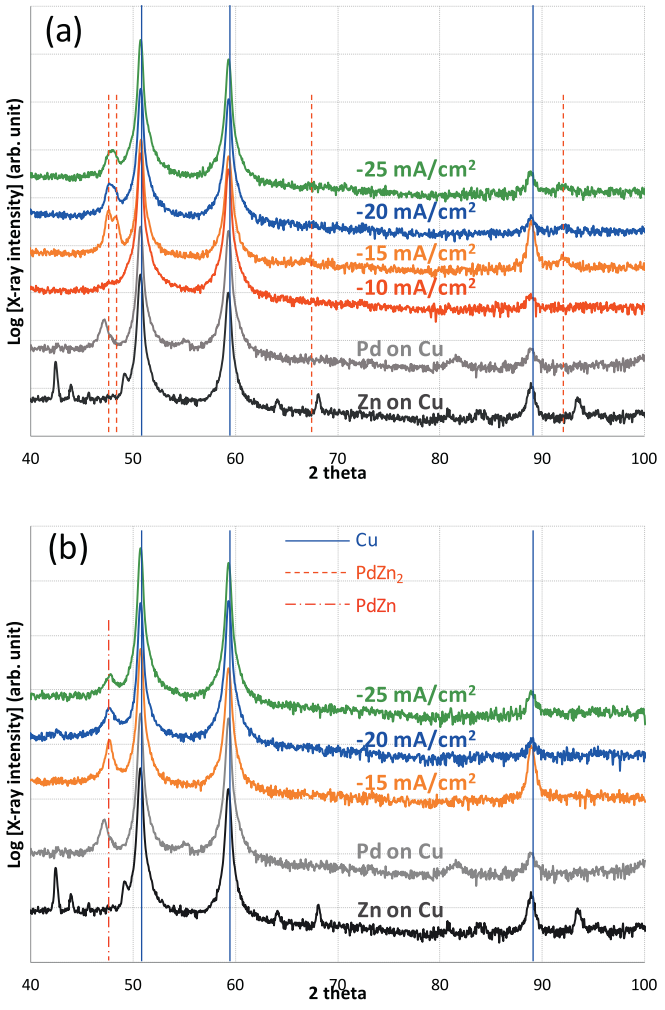

Fig. 7. XRD patterns of Pd-Zn alloy films deposited at −15, −20, and −25 mA/cm^2 (a) before and (b) after anodic stripping at −0.5 V. The XRD of pure Zn and pure Pd were also included.

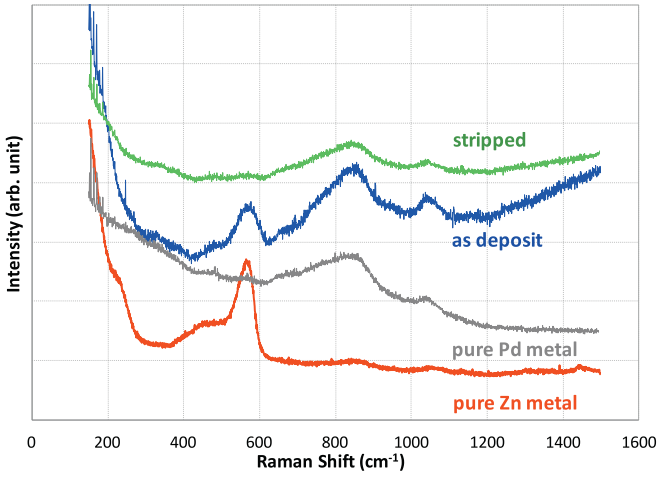

Fig. 8. Raman spectra of a Pd-Zn alloy film deposited at −25 mA/cm^2 before and after anodic stripping at −0.5 V. The spectra of pure Zn and pure Pd were included for comparison.

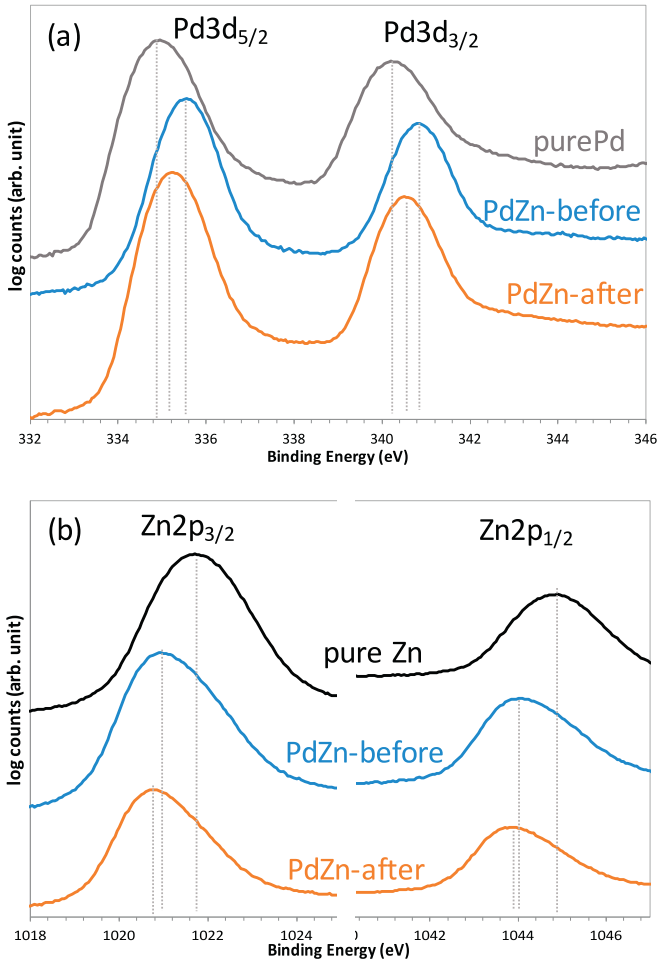

Fig. 9. (a) Pd3d and (b) Zn2p XPS spectra of a Pd-Zn alloy film deposited at −25 mA/cm^2 before and after anodic stripping at −0.5 V. The spectra of pure Zn and pure Pd were included for comparison.

0.31°), corresponding to an average grain size of 53, 24, and 27 nm for films originally deposited at −15, −20 and −25 mA/cm^2, respectively. These grain sizes are much smaller than the nodular features observed under SEM, suggesting that the nodules were agglomerates of multiple grains.

The alloy films were also characterized with Raman spectrum before and after stripping. The spectra were similar for the three films show in Fig. 7. Fig. 8 shows the spectra of a representative sample, which was prepared at −25 mA/cm^2. The spectra of pure Zn and pure Pd were included for comparison as well. The Raman peak at 560 cm^{-1} and the shoulder observed in the as-deposit sample results from a surface ZnO layer. The two broad and weak peaks at 840 and 1040 cm^{-1} observed for both Pd and alloy samples do not match for PdO spectrum [59] and are believed not to associate with the metal films. The spectra of alloy films before and after stripping are alike except for the ZnO peak. The absence of this vibration peak in the anodically stripped alloy is consistent with the removal of excessive Zn. More importantly, it also confirms that a stable PdZn bimetallic compound has formed and the Zn atoms in this compound is stabilized by Pd and does not get oxidized in air.

XPS spectra were also acquired for alloy films deposited at −25 mA/cm^2, before and after stripping. Fig. 9 shows the Pd 3d and Zn 2p XPS spectra of these films in comparison with the ones acquired from electrodeposited pure Pd and pure Zn films. A 30 s sputtering procedure was used immediately before the analysis to remove surface native oxides, if any. As shown in Fig. S4 in Supporting Materials, de-convolution of most XPS peaks resolves only one dominant Gaussian peak without or with a much less pronounced shoulder peak. Therefore, the spectra in Fig. 9 only show the overall peaks without de-convolution and were plotted in log scale of intensity for easier comparison. A shift

Table 1
XPS peak positions (in binding energy, eV) obtained from XPS spectra of pure Pd, pure Zn, as-deposited and anodically stripped Pd-Zn films. Values in parentheses are the binding energy in alloys as compared from pure metals.

Binding energy (eV)	Pd 3d 5/2	Pd 3d 3/2	Zn 2p 3/2	Zn 2p 1/2
Pure Pd	334.95	340.2		
Pure Zn			1021.7	1044.9
As-deposited	335.55	340.85	1020.95	1044.1
$Pd_{16}Zn_{84}$	(+0.6)	(+0.65)	(−0.75)	(−0.8)
Stripped $Pd_{50}Zn_{50}$	335.25	340.5	1020.75	1043.95
	(+0.3)	(+0.3)	(−0.95)	(−0.95)

toward higher binding energy of Pd and a shift toward lower binding energy for Zn were observed in the alloys, suggesting the formation of a strong bond between Pd and Zn where partial charge transfer can occur [60]. This is also consistent with the underpotential co-deposition discussed in the CV studies and the self-terminating behavior during anodic stripping.

Table 1 summarizes the peak positions as well as the shifts for alloys. It can be seen that the two peaks in any doublet always shift simultaneously. As compared with pure Pd film, the binding energy of Pd 3d core levels increase by about 0.6 and 0.3 eV in the as-deposited and stripped Pd-Zn alloys. On the other hand, the Zn 2p core levels decrease by about −0.8 and −0.95 eV in the as-deposited and stripped Pd-Zn alloys as compared with pure Zn. As discussed in Fig. 4, the compositions of the alloy films were $Pd_{16}Zn_{84}$ and $Pd_{50}Zn_{50}$ before and after stripping, respectively. In other words, the higher Zn content the more significant shifts in Pd 3d peaks, and the higher Pd content the stronger shifts in Zn 2p levels. These observations are consistent with the XPS studies on vapor deposited alloy specimens, where Pd and Zn in various amount equivalent up to a few monolayers were deposited [61].

4. Conclusion

Electrodeposition and anodic stripping of Pd-Zn binary alloys were investigated in an ammonia-citrate electrolyte. Electrodeposition of Zn was promoted in the presence of Pd due to the underpotential co-deposition. On the other hand, Pd deposition rate in alloy was lower than the elemental deposition, similar to the anomalous codeposition. Furthermore, a reversible adsorption and desorption of hydrogen was observed in CVs, where the amount of hydrogen was related to the palladium in the film. While Zn-rich alloys with various compositions were deposited at different current densities, bimetallic 1:1 PdZn compound was obtained after stripping. The crystallographic structure was also changed from orthorhombic $PdZn_2$ phase to tetragonal PdZn phase. XPS characterization showed a shift to higher binding energy for Pd3d and lower binding energy for Zn2p in alloys, consistent with the bimetallic compound formation. The stability of the PdZn compound was manifested as the self-termination of stripping, the unchanged composition upon further anodic stripping, as well as the absence of surface ZnO in Raman characterization.

Funding

This research is partially supported by National Science Foundation through a grant CMMI-1662332 and Research Grant Committee at University of Alabama through a grant RG-14741.

Acknowledgement

National Science Foundation is acknowledged for support through Grant CMMI-1662332. University of Alabama Research Grants Committee is acknowledged for support through a grant RG-14741. RJM thanks North Carolina State University for a travel support to present this research. The central analytical facility and the Engineering College spectroscopy facility at the University of Alabama are acknowledged for access to equipment used in film characterization in this project. Matthew Confer is acknowledged for Raman training. Engineering machine shop and glass shop at University of Alabama are acknowledged for making the parts used in this study.

Appendix A. Supplementary data

Supplementary data to this article can be found online at https://doi.org/10.1016/j.jelechem.2018.03.003.

References

[1] N. Shah, D. Panjala, G.P. Huffman, Hydrogen production by catalytic decomposition of methane, Energy Fuel 15 (6) (2001) 1528.
[2] S. Shen, T. Zhao, J. Xu, Y. Li, Synthesis of PdNi catalysts for the oxidation of ethanol in alkaline direct ethanol fuel cells, J. Power Sources 195 (4) (2010) 1001.
[3] Z. Qi, H. Geng, X. Wang, C. Zhao, H. Ji, C. Zhang, J. Xu, Z. Zhang, Novel nanocrystalline PdNi alloy catalyst for methanol and ethanol electro-oxidation in alkaline media, J. Power Sources 196 (14) (2011) 5823.
[4] A. Sarkany, Z. Zsoldos, B. Furlong, J. Hightower, L. Guczi, Hydrogenation of 1-butene and 1, 3-butadiene mixtures over Pd/ZnO catalysts, J. Catal. 141 (2) (1993) 566.
[5] P. Wehner, B. Gustafson, Catalytic hydrogenation of esters over Pd/ZnO, J. Catal. 135 (2) (1992) 420.
[6] M.W. Tew, H. Emerich, J.A. van Bokhoven, Formation and characterization of PdZn alloy: a very selective catalyst for alkyne semihydrogenation, J. Phys. Chem. C 115 (17) (2011) 8457.
[7] B. Green, C. Sass, L. Germinario, P. Wehner, B. Gustafson, Ester hydrogenation over Pd-Zn/SiO_2, J. Catal. 140 (2) (1993) 406.
[8] N. Iwasa, S. Masuda, N. Ogawa, N. Takezawa, Steam reforming of methanol over Pd/ZnO: effect of the formation of PdZn alloys upon the reaction, Appl. Catal. A Gen. 125 (1) (1995) 145.
[9] N. Iwasa, T. Mayanagi, N. Ogawa, K. Sakata, N. Takezawa, New catalytic functions of Pd–Zn, Pd–Ga, Pd–In, Pt–Zn, Pt–Ga and Pt–In alloys in the conversions of methanol, Catal. Lett. 54 (3) (1998) 119.
[10] N. Iwasa, T. Mayanagi, S. Masuda, N. Takezawa, Steam reforming of methanol over Pd-Zn catalysts, React. Kinet. Catal. Lett. 69 (2) (2000) 355.
[11] C. Rameshan, W. Stadlmayr, C. Weilach, S. Penner, H. Lorenz, M. Hävecker, R. Blume, T. Rocha, D. Teschner, A. Knop-Gericke, Subsurface-controlled CO_2 selectivity of PdZn near-surface alloys in H_2 generation by methanol steam reforming, Angew. Chem. Int. Ed. 49 (18) (2010) 3224.
[12] L.-Y. Hsieh, P.-K. Wang, C.-C. Chang, I.-W. Sun, Electrodeposition and dissolution of Zn on PdAg foil in a chlorozincate ionic liquid to fabricate micro-nanostructured PdAgZn alloy films for electrocatalysis, J. Electrochem. Soc. 164 (12) (2017) (D752).
[13] S.C. Hernandez, B.Y. Yoo, E. Stefanescu, S. Khizroe, N.V. Myung, Electrodeposition of iron-palladium thin films, Electrochim. Acta 53 (18) (2008) 5621.
[14] F.M. Takata, G. Pattanaik, W.A. Soffa, P.T. Sumodjo, G. Zangari, Synthesis of L1 0 Fe–Pd films by electrodeposition and thermal annealing, Electrochem. Commun. 10 (4) (2008) 568.
[15] Y. Xiao, G. Yu, J. Yuan, J. Wang, Z. Chen, Fabrication of Pd–Ni alloy nanowire arrays on HOPG surface by electrodeposition, Electrochim. Acta 51 (20) (2006) 4218.
[16] S.V. Kabanov, Y.P. Perelygin, Electrodeposition of palladium-zinc alloy from the ammonium chloride-Na(2)EDTA electrolyte, Russ. J. Appl. Chem. 74 (11) (2001) 1958.
[17] S.V. Kabanov, Y.P. Perelygin, Electrodeposition of palladium-zinc alloy from aminoacetic electrolyte, Russ. J. Appl. Chem. 75 (10) (2002) 1713.
[18] J.S. Wang, Z. Tan, T.Y. Mi, G.Q. Sun, Photoelectrochemistry of electrodeposited polycrystalline $CuInSe_2$ thin-films .1. Electrodeposition of $CuInSe_2$ films, Science in China Series B-Chemistry 35 (3) (1992) 281.
[19] Q.J. Xu, X.N. Deng, Oscillating behaviour on electrodeposited $CuInSe_2$ thin-films during H_2O_2 cathodic reduction, Acta Chim. Sin. 53 (11) (1995) 1076.
[20] R.N. Bhattacharya, A.M. Fernandez, M.A. Contreras, J. Keane, A.L. Tennant, K. Ramanathan, J.R. Tuttle, R.N. Noufi, A.M. Hermann, Electrodeposition of In-Se, Cu-Se, and Cu-In-Se thin films, J. Electrochem. Soc. 143 (3) (1996) 854.
[21] R.N. Bhattacharya, W. Batchelor, J.E. Granata, F. Hasoon, H. Wiesner, K. Ramanathan, J. Keane, R.N. Noufi, CuIn1-xGaxSe_2-based photovoltaic cells from electrodeposited and chemical bath deposited precursors, Sol. Energy Mater. Sol. Cells 55 (1–2) (1998) 83.
[22] A.M. Hermann, R. Westfall, R. Wind, Low-cost deposition of $CuInSe_2$ (CIS) films for CdS/CIS solar cells, Sol. Energy Mater. Sol. Cells 52 (3–4) (1998) 355.
[23] A.M. Fernandez, Preparation of Cu-In-Se precursor thin films by electrodeposition for the production of solar cells, Rev. Mex. Fis. 45 (1999) 58.
[24] Y.Q. Lai, F.Y. Liu, J. Yang, B. Wang, J. Li, Y.X. Liu, Photoelectrochemical behavior of electrodeposited CoSe thin films, Appl. Phys. Express 4 (7) (2011).
[25] Q. Huang, A.J. Kellock, S. Raoux, Electrodeposition of SbTe phase-change alloys, J. Electrochem. Soc. 155 (2) (2008) D104.
[26] G. Leimkuhler, I. Kerkamm, R. Reineke-Koch, Electrodeposition of antimony

telluride, J. Electrochem. Soc. 149 (10) (2002) C474.
[27] C. Jin, G. Zhang, T. Qian, X. Li, Z. Yao, Large-area Sb_2Te_3 nanowire arrays, J. Phys. Chem. B 109 (4) (2005) 1430.
[28] M. Panicker, M. Knaster, F. Kroger, Cathodic deposition of CdTe from aqueous electrolytes, J. Electrochem. Soc. 125 (4) (1978) 566.
[29] Y. Miyazaki, T. Kajitani, Preparation of Bi_2Te_3 films by electrodeposition, J. Cryst. Growth 229 (1) (2001) 542.
[30] M.S. Martin-Gonzalez, A.L. Prieto, R. Gronsky, T. Sands, A.M. Stacy, Insights into the electrodeposition of Bi_2Te_3, J. Electrochem. Soc. 149 (11) (2002) (C546).
[31] M.S. Sander, R. Gronsky, T. Sands, A.M. Stacy, Structure of bismuth telluride nanowire arrays fabricated by electrodeposition into porous anodic alumina templates, Chem. Mater. 15 (1) (2003) 335.
[32] K. Tittes, A. Bund, W. Plieth, A. Bentien, S. Paschen, M. Plotner, H. Grafe, W.J. Fischer, Electrochemical deposition of Bi_2Te_3 for thermoelectric microdevices, J. Solid State Electrochem. 7 (10) (2003) 714.
[33] A.P. Torane, C.D. Lokhande, P.S. Patil, C.H. Bhosale, Preparation and characterization of electrodeposited Bi_2Se_3 thin films, Mater. Chem. Phys. 55 (1) (1998) 51.
[34] J.D. Desai, Galvanostatic electrodeposition of Bi_2Se_3 thin films, Bull. Electrochem. 15 (7–8) (1999) 315.
[35] D. Kutyła, K. Kołczyk, P. Żabiński, R. Kowalik, Electrodeposition of Ni_3Se_2, J. Electrochem. Soc. 164 (12) (2017) D700.
[36] B.W. Gregory, J.L. Stickney, Electrochemical atomic layer epitaxy (Ecale), J. Electroanal. Chem. 300 (1–2) (1991) 543.
[37] D.W. Suggs, I. Villegas, B.W. Gregory, J.L. Stickney, Formation of compound semiconductors by electrochemical atomic layer epitaxy, J. Vac. Sci. Technol. A 10 (4) (1992) 886.
[38] L.P. Colletti, D. Teklay, J.L. Stickney, Thin-layer electrochemical studies of the oxidative underpotential deposition of sulfur and its application to the electrochemical atomic layer epitaxy deposition of Cds, J. Electroanal. Chem. 369 (1–2) (1994) 145.
[39] R. Vaidyanathan, J.L. Stickney, S.M. Cox, S.P. Compton, U. Happek, Formation of In_2Se_3 thin films and nanostructures using electrochemical atomic layer epitaxy, J. Electroanal. Chem. 559 (55) (2003).
[40] M.K. Mathe, S.M. Cox, B.H. Flowers, R. Vaidyanathan, L. Pham, N. Srisook, U. Happek, J.L. Stickney, Deposition of CdSe by EC-ALE, J. Cryst. Growth 271 (1–2) (2004) 55.
[41] V. Venkatasamy, I. Shao, Q. Huang, J.L. Stickney, ALD approach toward electrodeposition of Sb(2)Te(3) for phase-change memory applications, J. Electrochem. Soc. 155 (11) (2008) D693.
[42] J. Yang, W. Zhu, X. Gao, S. Bao, X. Fan, X. Duan, J. Hou, Formation and characterization of Sb_2Te_3 nanofilms on Pt by electrochemical atomic layer epitaxy, J. Phys. Chem. B 110 (10) (2006) 4599.
[43] S. Brankovic, J. Wang, R. Adžić, Metal monolayer deposition by replacement of metal adlayers on electrode surfaces, Surf. Sci. 474 (1) (2001) L173.
[44] D. Gokcen, Q. Yuan, S.R. Brankovic, Nucleation of Pt monolayers deposited via surface limited redox replacement reaction, J. Electrochem. Soc. 161 (7) (2014) D3051.
[45] E. Bulut, D. Wu, N. Dole, H. Kilic, S.R. Brankovic, Reaction kinetics of metal deposition via surface limited redox replacement of underpotentially deposited monolayer studied by surface reflectivity and open circuit potential measurements, J. Electrochem. Soc. 164 (4) (2017) D159.
[46] L. Yu, R. Akolkar, Lead underpotential deposition for the surface characterization of silver ad-atom modified gold electrocatalysts for glucose oxidation, J. Electroanal. Chem. 792 (2017) 61.
[47] K. Venkatraman, Y. Dordi, R. Akolkar, Electrochemical atomic layer deposition of cobalt enabled by the surface-limited redox replacement of underpotentially deposited zinc, J. Electrochem. Soc. 164 (2) (2017) D104.
[48] A.E. Martell, R.M. Smith, Critical Stability Constants, Plenum Press, New York, 1974.
[49] A.J. Bard, L.R. Faulkner, J. Leddy, C.G. Zoski, Electrochemical Methods: Fundamentals and Applications, 2 Wiley, New York, 1980.
[50] W.M. Haynes, CRC Handbook of Chemistry and Physics, 96th ed., CRC press, Boca Raton, FL, 2015.
[51] H. Dahms, I. Croll, The anomalous codeposition of iron-nickel alloys, J. Electrochem. Soc. 112 (8) (1965) 771.
[52] S. Swathirajan, Electrodeposition of zinc + nickel alloy phases and electrochemical stripping studies of the anomalous codeposition of zinc, J. Electroanal. Chem. Interfacial Electrochem. 221 (1–2) (1987) 211.
[53] M. Matlosz, Competitive adsorption effects in the electrodeposition of iron-nickel alloys, J. Electrochem. Soc. 140 (8) (1993) 2272.
[54] N. Zech, E. Podlaha, D. Landolt, Anomalous codeposition of iron group metals: I. Experimental results, J. Electrochem. Soc. 146 (8) (1999) 2886.
[55] D. Kolb, M. Przasnyski, H. Gerischer, Underpotential deposition of metals and work function differences, J. Electroanal. Chem. Interfacial Electrochem. 54 (1) (1974) 25.
[56] M. Nicol, H. Philip, Underpotential deposition and its relation to the anomalous deposition of metals in alloys, J. Electroanal. Chem. Interfacial Electrochem. 70 (2) (1976) 233.
[57] J. Mallett, W. Shao, D. Liang, G. Zangari, Underpotential codeposition of Cu–Au alloys, Electrochem. Solid-State Lett. 12 (8) (2009) (D57).
[58] T.B. Massalski, H. Okamoto, P. Subramanian, L. Kacprzak, W.W. Scott, Binary Alloy Phase Diagrams, American Society for Metals, Metals Park, OH, 1986.
[59] W. Weber, R. Baird, G. Graham, Raman investigation of palladium oxide, rhodium sesquioxide and palladium rhodium dioxide, J. Raman Spectrosc. 19 (4) (1988) 239.
[60] M. Friedrich, A. Ormeci, Y. Grin, M. Armbrüster, PdZn or ZnPd: charge transfer and Pd–Pd bonding as the driving force for the tetragonal distortion of the cubic crystal structure, Z. Anorg. Allg. Chem. 636 (9–10) (2010) 1735.
[61] J.A. Rodriguez, Interactions in bimetallic bonding: electronic and chemical properties of PdZn surfaces, J. Phys. Chem. 98 (22) (1994) 5758.